17th World Conference on Earthquake Engineering, 17WCEE
Sendai, Japan - September 13th to 18th 2020

FORMULATION OF FRAGILITY CURVES FOR PETROCHEMICAL PLANT COMPONENTS BASED ON SYNTHETIC GROUND MOTION RECORDS AND SURROGATE MODELING

G. Abbiati[(1)], R. Di Filippo[(2)], O. Sayginer[(3)], O. S. Bursi [(4)], Fabrizio Paolacci [(5)]

[(1)] *Assistant Prof., Department of Engineering, University of Aarhus, Aarhus, DENMARK, abbiati@eng.au.dk*
[(2)] *Ph.D., Department of Civ., Env. and Mech. Engineering, University of Trento, Trento, ITALY, rocco.difilippo@unitn.it*
[(3)] *Ph.D. Student. Department of Civ., Env. and Mech. Engineering, University of Trento, Trento, ITALY, osma.sayginer@unitn.it*
[(4)] *Full Professor, Department of Civ., Env. and Mech. Engineering, University of Trento, Trento, ITALY, oreste.bursi@unitn.it*
[(5)] *Ass. Professor, Department of Engineering, Roma Tre University, Rome, ITALY, fabrizio.paolacci@uniroma3.it*

Abstract

Seismic fragility analysis of petrochemical plants typically relies on finite element models for predicting the structural response given a set of hazard-consistent ground motion accelerograms. However, the lack of rigorous validation of computational models through systematic comparison with experiments and reduced number of hazard consistent ground motion records pose a severe limitation to the quantification of the structural response variability. In response to such a challenge, this paper outlines a procedure for seismic fragility analysis of petrochemical plants that relies on a stochastic model of the seismic input calibrated against a set of hazard-consistent site-specific accelerograms. Hierarchical kriging is used to surrogate the response of the petrochemical plant obtained from a set of computational models with different levels of fidelity and validated against hybrid simulations. Fragility curves or surfaces that relate one or multiple intensity measures, which correspond to a subset of the ground motion model parameters, to engineering demand parameters are obtained after the marginalization of kriging surrogates.

Keywords: performance-based earthquake engineering; fragility curve; synthetic ground motion; kriging surrogate modeling; tank-piping system.

1 Introduction

Industrial facilities like chemical, oil and gas plants can trigger severe environmental and human consequences when subjected to seismic action. Moreover, such consequences are not always limited to the facilities themselves but can possibly affect nearby communities, infrastructures and other plants. As a matter of fact, earthquakes can cause exceptional human and economic losses in the case of natural-technological (NaTech) events [1, 2]. Some recent examples of such events are petrochemical plant fires during the Izmint earthquake of 1999 [3], environmental chemical contaminations following the Sichuan earthquake of 2008 [4] and the nuclear and radiation accident caused by the 2011 Fukushima earthquake [5]. In order to prevent the severe consequences of NaTech events, the European directive Seveso-III (Directive 2012/18/EU) explicitly states that safety reports for industrial plants involving hazardous substances should include a “detailed description of the possible major-accident scenarios and their probability or the conditions under which they occur.”

Along this line, the performance-based engineering framework developed by the Pacific Earthquake Engineering Research (PEER) Center, namely the PEER framework [6], can be used to evaluate the structural performance and the associated risks. In detail, the PEER framework utilizes the following variables:

- Intensity Measure (IM), which quantifies the intensity of the hazard (e.g., peak ground acceleration).
- Engineering Demand Parameters (EDP), which quantifies the structural response of the structure (e.g., maximum displacement).
- Damage Measure (DM), which is an indicator of the state of a structural or non-structural component with respect to the ability of satisfying functionality requirements (e.g., fluid leakage).

- Decision Variables (DV), which describes consequences of damage (e.g., repairing costs or number of casualties).

In order to check the achievement of design objectives, the PEER integral expresses the conditional probability of exceeding a single (scalar) decision variable for a given hazard,

$$P(DV > dv|IM = im) = \int\int G_{DV|DM}(dv|dm)\left|dG_{DM|EDP}(dm|edp)\right|\left|dG_{EDP|IM}(edp|im)\right|$$

where $G_{X|Y}$ is referred to as a fragility curve and denotes the complementary cumulative distribution function of intermediate variable X (DV, DM, and EDP) conditioned on intermediate variable Y (DM, EDP, and IM). $\left|dG_{X|Y}\right|$ denotes the corresponding complementary probability density function. Lowercase variables imply individual realizations of their capitalized random variable counterparts. The PEER integral utilizes the total probability theorem to disaggregate the performance assessment into four intermediate probabilistic problems, namely, hazard, structural, vulnerability, and loss analysis carried out by independent working groups with complementary expertise. In detail, hazard analysis provides the value of the intensity measure corresponding to a hazard of given mean annual frequency of occurrence. The demand model $G_{EDP|IM}$ and the damage model $G_{DM|EDP}$ are the outcomes of the structural and the vulnerability analysis, respectively, and both involve the use of structural simulators. Finally, the decision model $G_{DV|DM}$ is the outcome of the loss analysis, which relies on building/repairing costs and post-disaster survey data. The extension of the PEER framework to other types of hazards (e.g., fire, wind, and blast) is a matter of ongoing research [7, 8, 9, 10]. However, as clearly highlighted by the opinion paper of Bradley [11], which advocates a methodological leap in seismic response analysis, 1) lack of rigorous validation of computational models through systematic comparison with experiments and 2) reduced number of hazard consistent ground motion records pose a severe limitation to the quantification of the structural response variability.

In response to such a challenge, this paper outlines a procedure for formulating demand models in the form of fragility curves for petrochemical plant components. The proposed method relies on a stochastic model of the seismic input calibrated against a set of hazard-consistent site-specific accelerograms and makes extensive use of surrogate modeling for merging evaluations of multi-fidelity computational simulators. The effectiveness of the proposed method is demonstrated for a realistic case study, which consists of a tank-piping system subjected to unidirectional ground motion excitation [12]. Structural performances are evaluated against loos-of-containment. In detail, probabilistic seismic hazard analysis (PSHA) [13] is performed to support the selection of site-specific ground motion accelerograms, which are used to calibrate the parameters of a stochastic model of the seismic input. The latter consists of a baseline noise vector subjected to a linear time-varying filter and a time modulating function mimicking frequency drifts and Husid plots of real records, respectively [14]. Hierarchical kriging is used to surrogate the response of the tank-piping system obtained from a set of computational models with different levels of fidelity and validated against hybrid simulations (HSs) [15]. Fragility curves or surfaces that relate one or multiple intensity measures (IMs), which correspond to a subset of the ground motion model parameters, to engineering demand parameters (EDPs) are obtained after the marginalization of kriging surrogates. A global sensitivity analysis of the structural response based on polynomial chaos expansion and Sobol' decomposition [16] is used to quantify the sufficiency of the selected IM vector [17].

2 Tank-piping system case study

The coupled tank-piping system under study is composed of a slender steel tank and a piping network connected through a bolted flange joint (BFJ), see . More specifically, the piping network consists of 8" (outer diameter: 219.08mm; thickness: 8.18mm) and 6" (outer diameter: 168.28mm; thickness: 7.11mm) schedule 40 straight pipes and contains two elbows, a bolted-flanged joint (BFJ) and a tee joint. The structural system is subjected to a uni-directional ground motion excitation.

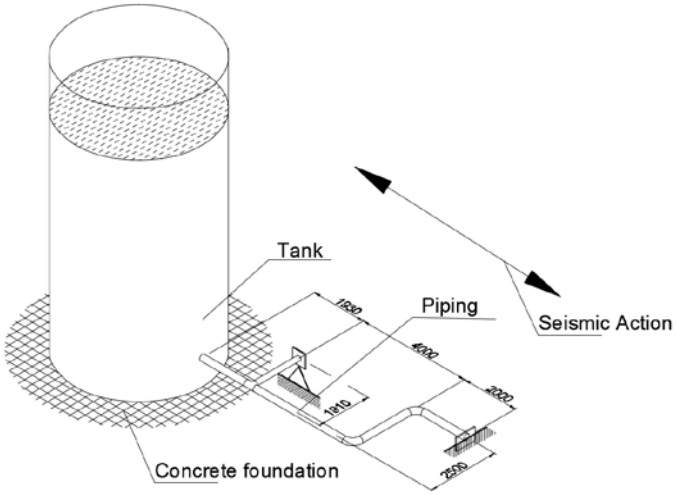

Fig. 1 – Realistic tank-piping system, measures in mm.

Both the adopted synthetic ground motion model and the numerical modelling of the structure, including the experimental validation based on Hs, are reported in the following subsections.

2.1 Synthetic ground motion model

In order to define the proper seismic input for the fragility analysis, the first step of this procedure is performing a PSHA [13], of a hypothetical location where our case study would be placed i.e., Hanford (CA, US). To do that, we relied on the United States Geological Survey (USGS) database and the relevant PSHA results are depicted in Fig. 2.

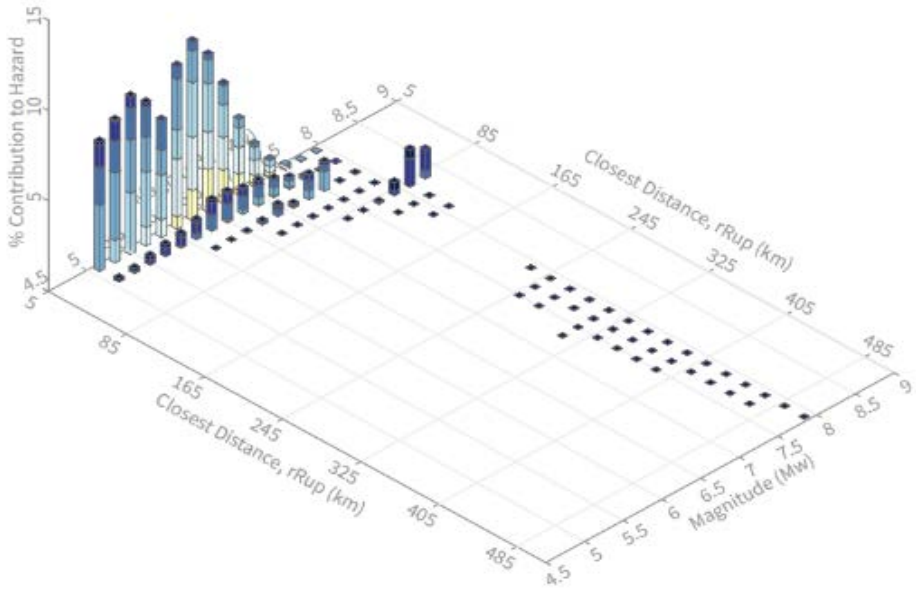

Fig. 2 – PSHA for Hanford, California (US).

From the deaggregation analysis, see for reference Fig. 2, we obtain the mode values for magnitude (M_w) and distance from the fault (R), which read 6.3 and 10.75 km, respectively. Thus, based on these two values, a set of 7 compatible accelerograms were selected, which are reported in Table 1.

Table 1 – Set of compatible accelerograms.

Earthquake Name	Station Name	M_w	Distance (km)
"Northridge-01"	"Canoga Park - Topanga Can"	6.69	14.7
"Northridge-01"	"Canyon Country - W Lost Cany"	6.69	12.44
"Northridge-01"	"N Hollywood - Coldwater Can"	6.69	12.51
"Northridge-01"	"Northridge - 17645 Saticoy "	6.69	12.09
"Northridge-01"	"Simi Valley - Katherine Rd"	6.69	13.42
"Northridge-01"	"Sun Valley - Roscoe Blvd"	6.69	10.05
"Northridge01"	"Sunland - Mt Gleason Ave"	6.69	13.35
"Northridge02"	"Pacoima Kagel Canyon"	6.05	11.34

As reported in Table 1, all the different records are related to the Northridge earthquake, as downloaded from the NGA database [18]. For each record, we calibrated the six parameters reported in Table 2 of the stochastic ground motion model (SGM) proposed by Rezaian and Der Kiureghian [14], which reads,

$$a_g(t) = q(t,\boldsymbol{\alpha})\left[\frac{1}{\sigma_f(t)}\int_{-\infty}^{t} h\big(t-\tau,\boldsymbol{\lambda}(\tau)\big)\omega(\tau)d\tau\right] \tag{1}$$

where $q(t,\boldsymbol{\alpha})$ is the time modulating function:

$$\begin{cases} q(t,\boldsymbol{\alpha}) = 0 & if\ t \le 0 \\ q(t,\boldsymbol{\alpha}) = \alpha_1 t^{\alpha_2 - 1} exp(-\alpha_3 t) & if\ t < 0 \end{cases} \tag{2}$$

with $\hat{\boldsymbol{\alpha}}$ defined by means of:

$$\hat{\boldsymbol{\alpha}} = arg\min_{\boldsymbol{\alpha}}\left(\left|I_a(t_{45}) - \hat{I}_a(t_{45})\right| + \left|I_a(t_{95}) - \hat{I}_a(t_{95})\right|\right) \tag{3}$$

Moreover, $\omega(\tau)$ is the baseline noise and $h\big(t-\tau,\boldsymbol{\lambda}(\tau)\big)$ is the impulse response function of a linear time-varying filter, that can be expressed as follows:

$$h\big(t-\tau,\boldsymbol{\lambda}(\tau)\big) = f(\omega_f,\zeta_f) \tag{4}$$

$$\omega_f = \omega_{mid} + \omega'(t - t_{mid}) \tag{5}$$

Table 2 – Stochastic ground motion model parameters.

Parameter	**Description**
I_a	Arias intensity
$D_{5\text{-}95}$	Time interval of 95% of the I_a
t_{mid}	Time at which 45% of the I_a is reached
ω_{mid}	Filter frequency at t_{mid}
ζ_f,	Filter damping ratio (constant).
ω'	Rate of change of the filter frequency with time

Following the calibration process described in [14], we calibrate the model parameters for each ground motion record reported in Table 1. As a result, Table 3 summarizes the outcomes of the calibration procedure.

Table 3 – Parameters distributions

Name	Distribution	LB	UB	Units
I_a	Uniform	0.019	3.992	m^2/s^3
D_{5-95}	Uniform	5.083	16.810	s
T_{45}	Uniform	1.596	5.664	s
ω_{mid}	Uniform	14.620	31.000	rad/s
ζ	Uniform	0.074	0.557	-

The idea behind using records from a single event is to formulate a site-specific seismic input model. The range of calibrated parameter values determines a context of interest where unbiased fragility curves are sought.

2.2 *Low- and high-fidelity computational models*

Additional details can be found in [19]. Two finite-element models with different degrees of fidelity were implemented and calibrated against HS experiments, namely a high-fidelity (HF) model, which was implemented in ANSYS, and a low-fidelity (LF) model, which was implemented in MATLAB. The same simplified 3-DoFs tank model depicted in Fig. 3 was used for both LF and HF models [20]. Related parameters are reported in Table 4.

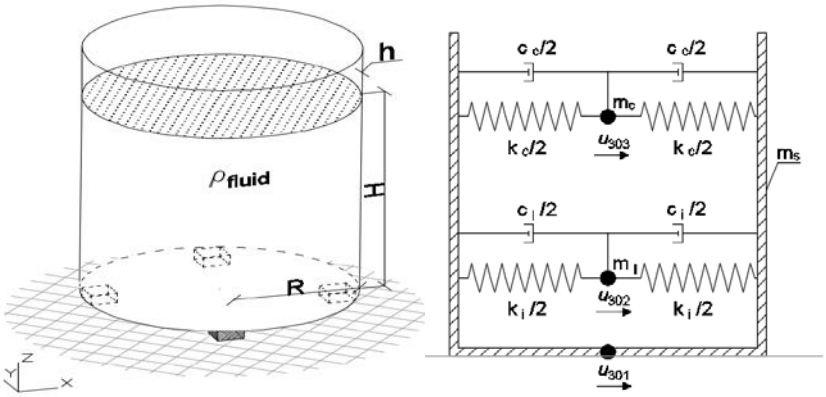

Fig. 3 – Simplified tank model after [20].

Table 4 – Simplified tank model parameters.

Parameter	Value	Unit
E	210	GPa
H	12	M
h	2	M
R	4	M
ρ_{fluid}	900	kg/m^3
m_c – convective mass	7.98e+4	Kg
m_i – impulsive mass	5.47e+5	Kg

A nonlinear Mostaghel spring [21] was used to simulate the shear response of seismic isolators. The main equations of the Mostaghel model read,

$$\begin{cases} \dot{r} = \left(\alpha_{MST} k_{MST} + (1-\alpha_{MST}) k_{MST} \left(\bar{N}(v)\bar{M}(s-\delta_{MST}) + M(v)N(s+\delta_{MST})\right)\right) v \\ \dot{u} = v \end{cases} \tag{6}$$

Where, the parameter s and the remaining functions $N, M, \bar{N}$ and $\bar{M}$ are defined as follows:

$$s = \frac{r - \alpha_{MST} k_{MST} u}{(1-\alpha_{MST}) k_{MST}} \tag{7}$$

$$\begin{gathered} N(v) = 0.5\big(1 + sgn(v)\big)\Big(1 + \big(1 - sgn(v)\big)\Big) \\ M(v) = 1 - N(v) \\ \bar{N}(v) = M(-v) \\ \bar{M}(v) + N(-v) \end{gathered} \tag{8}$$

The parameters k_{MST}, α_{MST} and δ_{MST} represent initial stiffness, post-yielding stiffness reduction factor and yielding displacement of the idealized spring system. These parameters are set in order to replicate the static friction phenomenon:

$$\begin{gathered} \delta_{MST} = \Delta = 1e-3\ m \\ \alpha_{MST} = 1e-3 \\ k_{MST} = \frac{\mu(m_l + m_t)g}{\Delta} = 2.18e+8 \frac{N}{m} \end{gathered} \tag{9}$$

With regard to the LF model, pipe elbows were modeled as equivalent linear beams and the relevant scheme is shown in Fig. 4. Further details can be found in [19].

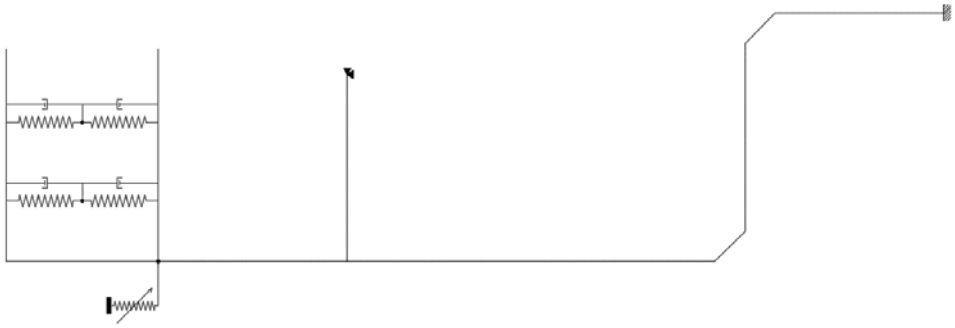

Fig. 4 – Scheme of the low-fidelity model.

After this process of calibration against experimental results, the performances of the LF model are assessed against the unbiased results from the HS.

Differently from the LF model, shell-based elbows endowed with a non-linear constitutive law for the API 5L X52 steel were employed [19]. Fig. 5 provides an overview of the HF model implemented in ANSYS and took 300 sec for a single analysis.

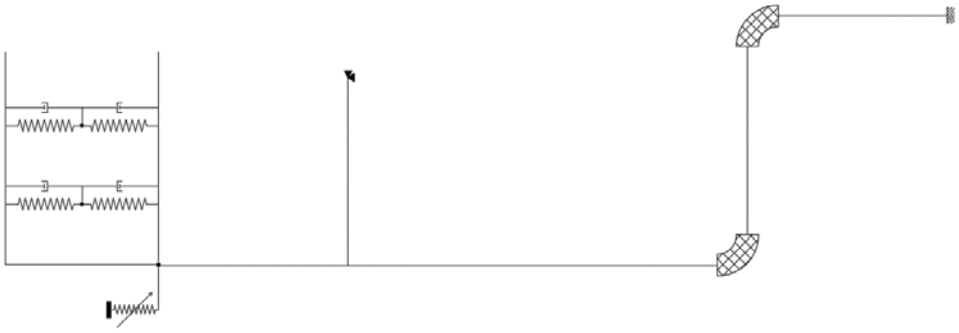

Fig. 5 – Scheme of the high-fidelity model.

It is important to remark that for each sample of the input parameters i.e., IMs, the baseline noise determines a set of synthetic ground motion records. Therefore, the 90% quantiles of hoop-strain peaks are selected as EDPs for the fragility analysis. These quantities are indicated as $\epsilon_{elb1,0.90}$ and $\epsilon_{elb2,0.90}$, and must be distinguished from single record evaluations ϵ_{elb1} and ϵ_{elb2}.

2.3 Model validation based on hybrid simulation

In order to validate both LF and HF models, a hybrid simulation (HS) campaign was performed at the University of Trento, Italy. In detail, the tank-piping system was partitioned into a numerical substructure (NS), which includes the tank provided with seismic isolators, and a physical substructure (PS), which comprises the piping network. The hybrid model of the tank-piping system is depicted in Fig. 6. For additional information, the reader can refer to [19].

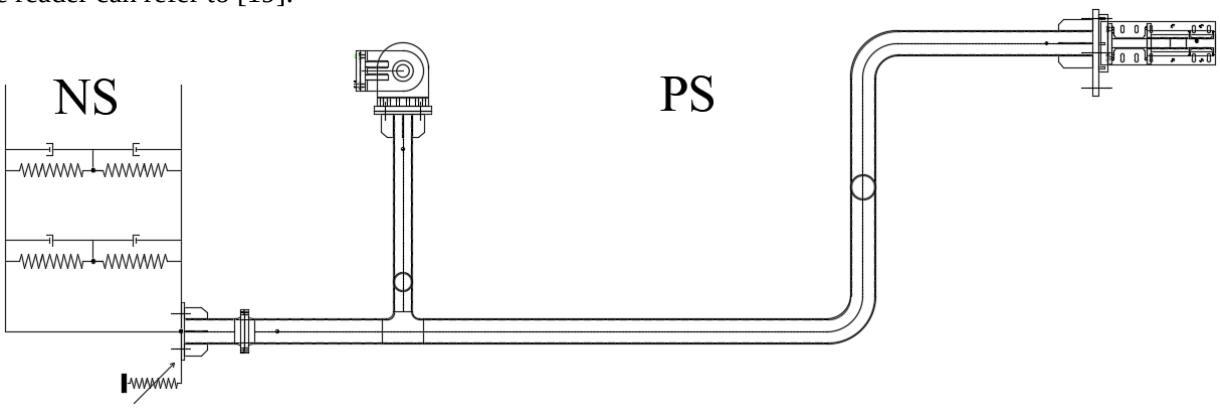

Fig. 6 – Hybrid simulator scheme.

The experimental setup of the PS is shown in Fig. 7. As can be appreciated from the figure, a hydraulic actuator of 250 kN force capacity control the interface displacement of the physical piping system. The piping network was filled with 15 bar pressured water. A set strain gauges (SGs) measured the hoop strain of each elbow, which is a reliable good indicator of the damage level [22].

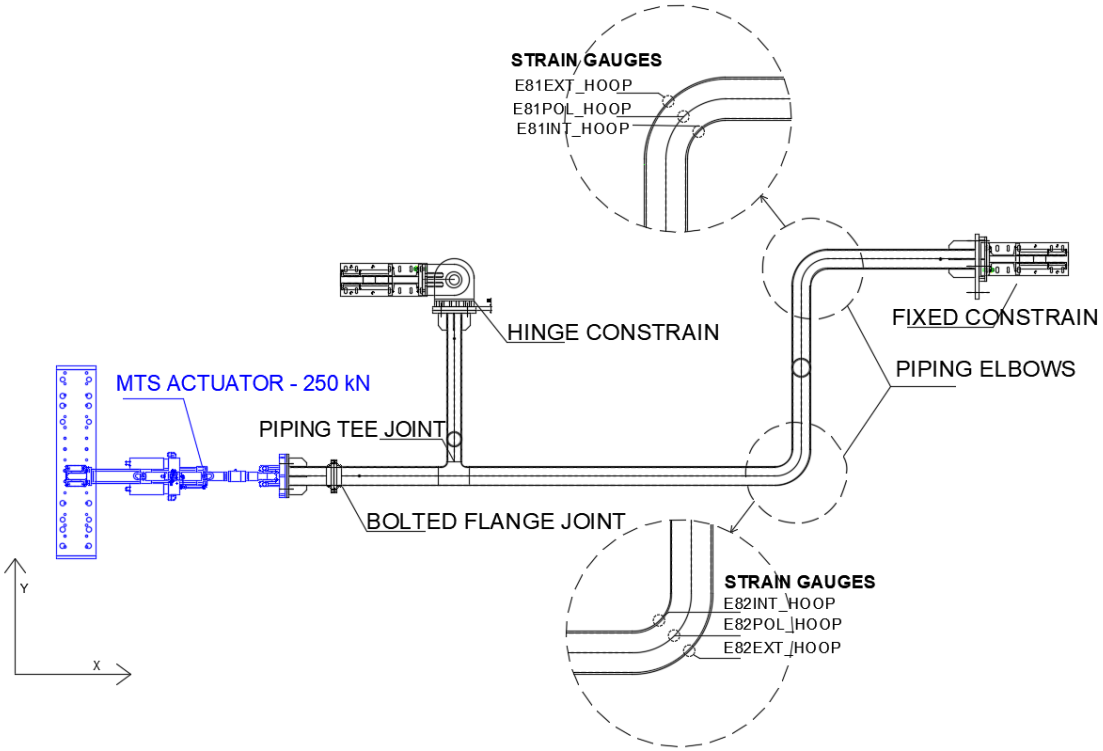

Fig. 7 – Experimental setup and sensor placement.

HSs were conducted considering seven synthetic records generated from the SGM model described in Section 2.1. Four records were selected in order to keep the piping response in the linear regime i.e., serviceability limit state (SLS) whereas the other three were expected to induce a nonlinear structural response of the piping system i.e., ultimate limit state (ULS). Both corresponding limit state functions were defined with respect to the tank sliding displacement, u_{max}, with $u_{max} < 0.04\ m$ for SLS signals and $u_{max} > 0.06\ m$ for ULS ones, see Fig. 8 for the relevant spectral accelerations.

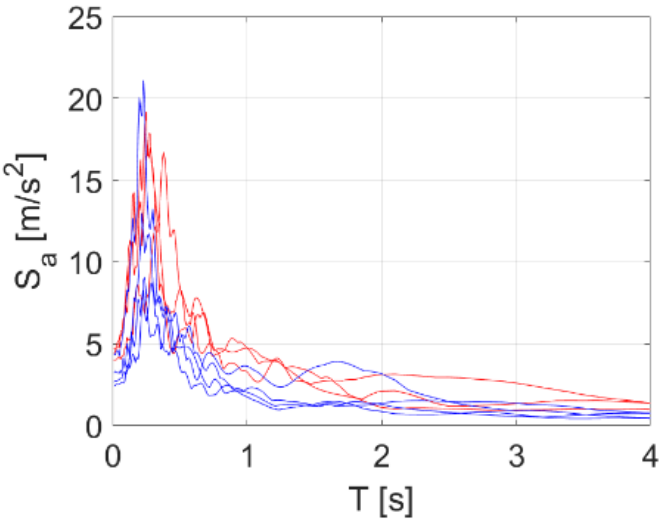

Fig. 8 – Spectral accelerations of synthetic ground motions

As it is possible to notice from Fig. 8, even with a relatively small number of signals, the selected set offers a significant ground motion variability. A total of seven HSs were performed with a testing time scale equal to 64.

Fig. 9 and Fig. 10 compare the hoop strain histories of Elbow #1 $\epsilon_{elb,1}$ measured from HS and predicted by the calibrated LF and HF models, respectively.

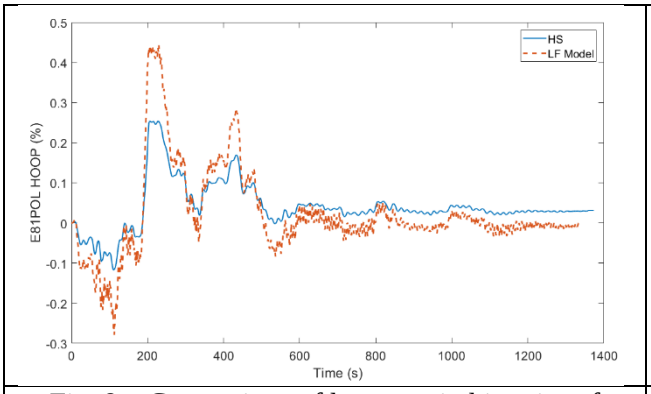

Fig. 9 – Comparison of hoop strain histories of elbow #1 measured from HS and predicted by the calibrated LF model.

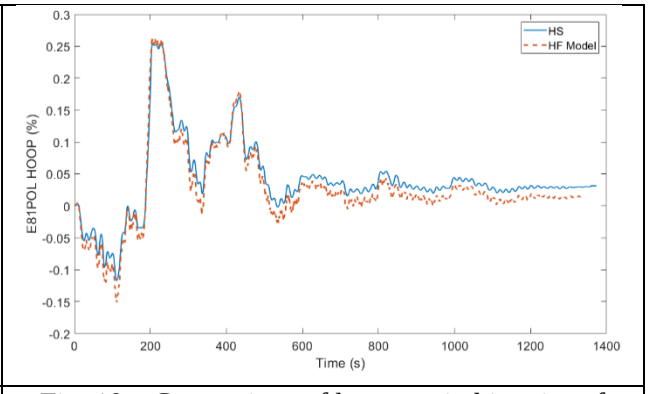

Fig. 10 – Comparison of hoop strain histories of elbow #1 measured from HS and predicted by the calibrated HF model.

Fig. 9 highlights that the LF model is capable of predicting the time history of the experimental strain even though an offset is present. However, each LF model simulation takes about 20 seconds on a standard personal computer. Fig. 10 highlights a satisfactory matching between the HS and the HF model. It is clear that, despite a higher requirement of computational power, the HF model outperforms the LF.

3 Seismic fragility analysis of the tank-piping system

3.1 Basics of hierarchical Kriging

The Kriging method is a well-known technique to build surrogate model considering the output of a generic simulator as a realization of a Gaussian process [23]:

$$y = \mathcal{M}(\boldsymbol{x}) \approx \boldsymbol{\beta}^T \boldsymbol{f}(\boldsymbol{x}) + \sigma_y^2 Z(\boldsymbol{x}, \omega) \tag{10}$$

where $\boldsymbol{f}(\boldsymbol{x}) = [f_1(\boldsymbol{x}), \dots, f_p(\boldsymbol{x})]$ is a column vector of regression functions of a generic point $\boldsymbol{x}$ of the input parameter space $\mathcal{D}_X$ and $\boldsymbol{\beta}$ is a column vector of coefficients. Their product forms the trend of a Gaussian process of variance σ_y^2; $Z(\boldsymbol{x}, \omega)$ is a zero-mean, unit-variance, stationary Gaussian process, which is characterized by an autocorrelation function $R(|\boldsymbol{x} - \boldsymbol{x}'|; \boldsymbol{\rho})$ and its hyper-parameters $\boldsymbol{\rho}$. The Kriging surrogate is trained with a set of realizations $\boldsymbol{X} = \{\boldsymbol{x}^{(i)}, i = 1, \dots, N_t\}$ on the input parameter space $\mathcal{D}_X$ and the corresponding responses of the computational model $\boldsymbol{Y} = \{y^{(i)} = \mathcal{M}(\boldsymbol{x}^{(i)}), i = 1, \dots, N_t\}$, which together form the so-called Experimental Design (ED) $\{\boldsymbol{X}, \boldsymbol{Y}\}$. Having determined the Kriging parameters, the prediction value of the simulator output at a point $\boldsymbol{x} \in \mathcal{D}_X$ is a Gaussian variable with the following mean value and variance:

$$\mu_{\hat{Y}}(\boldsymbol{x}) = \boldsymbol{f}(\boldsymbol{x})^T \boldsymbol{\beta} + \boldsymbol{r}(\boldsymbol{x})^T \mathbf{R}^{-1}(\boldsymbol{Y} - \mathbf{F}\boldsymbol{\beta}) \tag{11}$$

$$\sigma_{\hat{Y}}(\boldsymbol{x}) = \sigma_y^2 (1 - \boldsymbol{r}(\boldsymbol{x})^T \mathbf{R}^{-1} \boldsymbol{r}(\boldsymbol{x}) + \boldsymbol{u}(\boldsymbol{x})^T (\mathbf{F}^T \mathbf{R}^{-1} \mathbf{F})^{-1} \boldsymbol{u}(\boldsymbol{x})) \tag{12}$$

where $r_i(\boldsymbol{x}) = R(|\boldsymbol{x} - \boldsymbol{x}^{(i)}|; \boldsymbol{\rho})$ and $\boldsymbol{u}(\boldsymbol{x}) = \mathbf{F}^T \mathbf{R}^{-1} \boldsymbol{r}(\boldsymbol{x}) - \boldsymbol{f}(\boldsymbol{x})$. Now, let's consider l simulators of increasing fidelity proportional to the evaluation cost. We denote by y_s the output of the simulator with the

highest level of fidelity. For any given level $1 \leq l \leq s$, hierarchical Kriging mean and variance predictors at an unobserved point $\boldsymbol{x}$ can be written as:

$$\mu_{\hat{Y}_l}(\boldsymbol{x}) = \mu_{\hat{Y}_{l-1}}(\boldsymbol{x})^T\beta + \boldsymbol{r}(\boldsymbol{x})^T\mathbf{R}^{-1}(\boldsymbol{Y}_l - \mathbf{F}\beta) \quad (13)$$

$$\sigma_{\hat{Y}_l}(\boldsymbol{x}) = \sigma_y^2(1 - \boldsymbol{r}(\boldsymbol{x})^T\mathbf{R}^{-1}\boldsymbol{r}(\boldsymbol{x}) + u(\boldsymbol{x})^T(\mathbf{F}^T\mathbf{R}^{-1}\mathbf{F})^{-1}u(\boldsymbol{x})) \quad (14)$$

where $r_i(\boldsymbol{x}) = R\left(\left|\boldsymbol{x} - \boldsymbol{x}^{(i)}\right|; \boldsymbol{\rho}\right)$ and $u(\boldsymbol{x}) = \mathbf{F}^T\mathbf{R}^{-1}\boldsymbol{r}(\boldsymbol{x}) - \mu_{\hat{Y}_{l-1}}(\boldsymbol{x})$ with $[\mathbf{F}]_i = \mu_{\hat{Y}_{l-1}}(\boldsymbol{x}^{(i)})$; $\boldsymbol{Y}_l$ is the vector of simulator l outputs, β is a regression factor (scaling). We note the similarity of the expressions in Eqs. (11-12) and Eqs. (13-14) where the Kriging mean predictor $\mu_{\hat{Y}_{l-1}}(\boldsymbol{x})$ of the lower fidelity simulator of index $l-1$ replaces $\boldsymbol{f}(\boldsymbol{x})$ as trend of the Kriging surrogate at level l. It is noteworthy that $\mathbf{R}^{-1}(\boldsymbol{Y}_l - \mathbf{F}\beta)$ depends only on data sampled by simulator l and, therefore, ED at various fidelity levels can be arbitrarily defined, that is, it is not required $\boldsymbol{X}_l$ to be a subset of $\boldsymbol{X}_{l-1}$. This formulation offers several other advantages. It is computationally cheap: we perform one Kriging estimation per fidelity level l. It is flexible in terms of how the Kriging surrogates are derived: since we perform one Kriging estimation per fidelity level l, the Kriging surrogates may be defined by different correlation kernels [15].

3.2 Formulation of fragility curves

As found in [19], three parameters I_a, ω_{mid} and ζ of the ground motion model determines almost the entire variance of the 90% quantiles of the peak values of the hoop-strains of Elbows #1 and #2, which was evaluated considering 200 realizations of baseline noise of a given sample of ground motion parameters. This was found to be enough to assure the seismic response convergence [19]. Thus, these three parameters are chosen to vary according to the statistical distributions defined in Table 3, while the remaining three are fixed at their average value with $D_{5\text{-}95}$ = 10.441 s, T_{45} = 3.7 s and ω' = -0.568 rad/s^2. In our case the input and output parameters are,

$$\boldsymbol{X} = \{I_a, \omega_{mid}, \zeta\}, \boldsymbol{Y} = \{\varepsilon_{elb1,0.90}, \varepsilon_{elb2,0.90}\}$$

A Kriging surrogate of the LF model was trained considering 200 samples of the synthetic ground motion model parameters obtained from a Sobol' sequence. Then, a hierarchical Kriging surrogate was trained considering the response of the HF model evaluated for the first 20 samples of the synthetic ground motion parameters using the Kriging surrogate of the LF model as trend function.

In order to perform a fragility analysis, we set two different limit states: i) a yielding limit state characterized by 0.17% hoop-strain peak, ii) an ECA limit state characterized by 0.47% hoop-strain peak, according to [24]. Finally, we perform a reliability analysis based on the results of a Monte Carlo sampling of the hierarchical Kriging surrogate response. According to the global sensitivity analysis reported in [19], Arias intensity I_a explains the largest portion of the variance of selected output response quantities. Therefore, fragility curves are obtained by the marginalization of hierarchical Kriging surrogates with respect to the remaining input parameters ω_{mid} and ζ. In Fig. 11 we show the relevant fragility curves of one of the two elbows regarding the I_a for both the limit states. Three curves are depicted to show the 95% probability confidence interval.

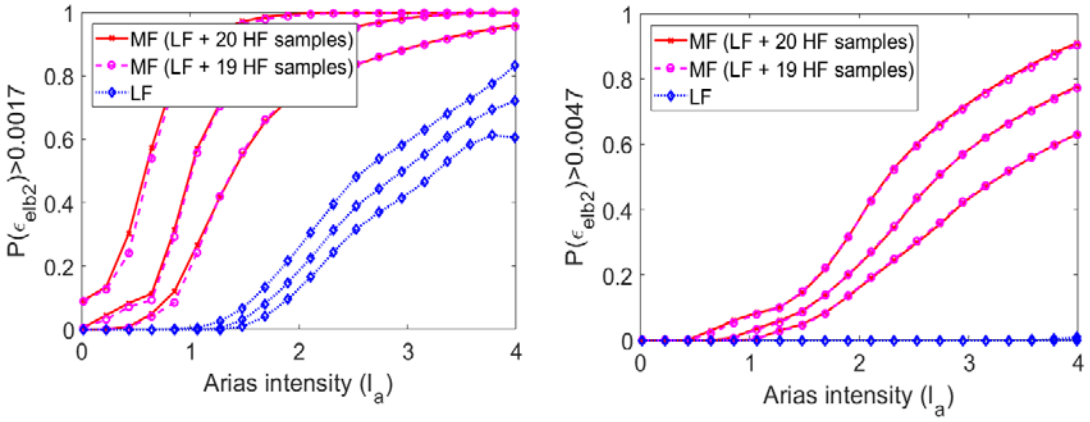

Fig. 11 – Elbow fragility curves for yielding (left) and ECA (right) limit state

From Fig. 11 it is possible to notice that the probabilities evaluated with 19 and 20 parameters realizations for the HF are almost equal, assuring the convergence of the curves. Moreover, the added value of the MF, enriched by HF results, offers a clear accuracy benefit over the biased LF simulator.

4 Conclusions

This paper outlines a procedure for formulating demand models in the form of fragility curves for petrochemical plant components. The proposed method relies on a stochastic model of the seismic input calibrated against a set of hazard-consistent site-specific accelerograms and makes use of hierarchical kriging surrogate modeling for merging evaluations of multi-fidelity computational simulators. The effectiveness of the proposed method is demonstrated for a realistic case study, which consists of a tank-piping system subjected to unidirectional ground motion excitation. Fragility curves computed via marginalization of kriging surrogates showed stable convergence with a limited number of HF model evaluation.

5 Acknowledgments

The authors greatly acknowledge Dr. Marco Broccardo (University of Liverpool) and Dr. Imad Abdallah (ETH Zurich) for their feedback on the proposed method.

6 References

[1] M. A. Cruz., L. J. Steinberg and A. L. Vetere-Arellano, "Emerging Issues for Natech Disaster Risk Management in Europe," *Journal of Risk Research*, vol. 9, no. 5, pp. 483-501,, 2006.

[2] L. Steinberg, H. Sengul and A. Cruz, "Natech Risk and Management: An Assessment of the State of the Art," *Natural Hazards*, vol. 46, pp. 143-152, 2008.

[3] H. Sezen and A. Whittaker, "Seismic Performance of Industrial Facilities Affected by the 1999 Turkey Earthquake," *Journal of Performance of Constructed Facilities*, vol. 20, no. 1, pp. 28-36, 2006.

[4] E. Krausmann, A. M. Cruz and B. Affeltranger, "The impact of the 12 May 2008 Wenchuan Earthquake on Industrial Facilities," *Journal of Loss Prevention in the Process Industries*, vol. 23, no. 2, pp. 242-248, 2010.

[5] P. Lipscy, K. Kushida and T. Incerti, "The Fukushima Disaster and Japan's Nuclear Plant Vulnerability in Comparative Perspective," *Environmental Science & Technology*, vol. 47, no. 12, p. 6082–6088, 2000.

[6] C. A. Cornell and H. Krawinkler, "Progress and challenges in seismic performance assessment," *PEER Center News*, vol. 3, no. 2, pp. 1-2, 2000.

[7] M. Barbato, F. Petrini, V. U. Unnikrishnan and M. Ciampoli, "Performance-Based Hurricane Engineering (PBHE) framework," *Structural Safety*, vol. 45, pp. 24-35, 2013.

[8] N. Attary, V. U. Unnikrishnan, J. W. van de Lindt, D. T. Cox and A. R. Barbosa, "Performance-Based Tsunami Engineering methodology for risk assessment of structures," *Engineering Structures*, vol. 141, pp. 676-686, 2017.

[9] D. Lange, S. Devaney and A. Usmani, "An application of the PEER performance based earthquake engineering framework to structures in fire," *Engineering Structures*, vol. 66, pp. 100-115, 2014.

[10] M. Ciampoli and F. Petrini, "Performance-based Aeolian risk assessment and reduction for tall buildings," *Probabilistic Engineering Mechanics*, vol. 28, pp. 75-84, 2012.

[11] B. A. Bradley, "A critical examination of seismic response uncertainty analysis in earthquake engineering," *Earthquake Engineering & Structural Dynamics*, vol. 42, no. 11, pp. 1717-1729, 2013.

[12] O. S. Bursi, R. di Filippo and others, *Component Fragility Evaluation, Seismic Safety Assessment and Design of Petrochemical Plants Under Design-Basis and Beyond-Design-Basis Accident Conditions, Final Report, INDUSE-2-SAFETY Project, Contr. No: RFS-PR-13056, Research Fund for Coal and Steel,*, 2018.

[13] P. Bazzurro and C. A. Cornell, "Disaggregation of seismic hazard," *Bulletin of the Seismological Society of America*, vol. 89, no. 2, p. 501–520, 1999.

[14] R. S. and D. K. A., "Simulation of synthetic ground motions for specified earthquake and site characteristics," *Earthquake Engineering & Structural Dynamics*, vol. 39, p. 1155–1180, 2010.

[15] I. Abdallah, C. Lataniotis and B. Sudret, "Parametric hierarchical kriging for multi-fidelity aero-servo-elastic simulators — Application to extreme loads on wind turbines.," *Probabilistic Engineering Mechanics*, vol. 55, pp. 67-77, 2018.

[16] B. Sudret, "Global sensitivity analysis using polynomial chaos expansions," *Reliability Engineering & System Safety*, vol. 93, no. 7, p. 964–979, 2008.

[17] F. Jalayer, J. L. Beck, M. Asce, F. Zareian and M. Asce, "Analyzing the Sufficiency of Alternative Scalar and Vector Intensity Measures of Ground Shaking Based on Information Theory.," *Journal of Engineering Mechanics*, vol. 138, no. 3, pp. 307-316, 2012.

[18] PEER Pacific Earthquake Engineering Research (PEER) Center, *Ground Motion Database*, May 24, 2016.

[19] R. di Filippo, G. Abbiati, O. Sayginer, P. Covi, O. Bursi and F. Paolacci, "Numerical surrogate model of a coupled tank-piping system for seismic fragility analysis with synthetic ground motions," in *PVP2019*, San Antonio, Texas, US., July 14-19, 2019.

[20] P. K. Malhotra, T. Wenk and M. Wieland, "Simple Procedure for Seismic Analysis of Liquid-Storage Tanks," *Structural Engineering International*, vol. 3, pp. 197-201, 2000.

[21] N. Mostaghel, "Analytical Description of Pinching, Degrading Hysteretic Systems," *Journal of Engineering Mechanics*, vol. 125, no. 2, pp. 216-224, 1999.

[22] O. S. Bursi, R. di Filippo, V. La Salandra, M. Pedot and M. S. Reza, "Probabilistic seismic analysis of an LNG subplant," *Journal of Loss Prevention in the Process Industry*, vol. 53, pp. 45-60, 2018.

[23] T. J. Santner, B. Williams and W. Notz, "The design and analysis of computer experiments," *Springer Science & Business Media*, 2013.

[24] DNV Det Norske Veritas, *DNV-OS-F101 Submarine Pipeline Systems*, 2000.

